https://doi.org/10.5194/acp-2022-219
Preprint. Discussion started: 22 April 2022

Atmospheric Chemistry and Physics
Discussions

Long-term variation study of fine-mode particle size and regional characteristics using AERONET data

Juseon Shin[1], Juhyeon Sim[1], Naghmeh Dehkhoda[1], Sohee Joo[1], Taekyung Kim[1], Gahyung Kim[1], Detlef Müller[2], Matthias Tesche[3], Sungkyun Shin[4], Dongho Shin[5], Youngmin Noh[6,*]

[1]Division of Earth Environmental System Science, Pukyong National University, Busan, Republic of Korea
[2] University of Hertfordshire, United Kingdom
[3] Leipzig Institute for Meteorology, Leipzig University, Leipzig, Germany
[4] Department of Atmospheric Particulate Matter Research, Seoul Institute of Technology, Seoul, Republic of Korea
[5] Fine Dust Research Department, Korea Institute of Energy Research, Daejeon, Republic of Korea
[6] Department of Environmental Engineer, Pukyong National University, Busan, Republic of Korea

Correspondence to: Youngmin Noh (nym@pknu.ac.kr)

Department of Environmental Engineering, Pukyong National University, Busan, Republic of Korea

Tel: +82-10-3222-3203

https://doi.org/10.5194/acp-2022-219
Preprint. Discussion started: 22 April 2022

Abstract. To identify the long-term trend of particle size variation, we analyzed aerosol optical depth (AOD, τ) separated as dust (τ_D) and coarse-(τ_{PC}) and fine-pollution particles (τ_{PF}) depending on emission sources and size. Ångström Exponent values are also identified separately as total and fine-mode particles (α_T and α_{PF}). We checked these trends in various ways; 1) first-order linear regression analysis of the annual average values, 2) percent variation using the slope of linear regression method, and 3) a reliability analysis using the Mann-Kendall (MK) test. We selected 17 AERONET sun/sky radiometer sites classified into six regions, i.e., Europe, North Africa, the Middle East, India, Southeast Asia, and Northeast Asia. τ decreased in Europe and Asian regions and increased in the Middle East, India, and North Africa. Values of τ_{PC} and τ_{PF}, show that aerosol loading caused by non-dust aerosols decreased in Europe and Asia and increased in India. In particular, τ_{PF} considerably decreased in Europe and Northeast Asia (95 % confidential levels in MK-test), and τ_{PC} decreased in Northeast Asia (Z-values for Seoul and Osaka are -2.95 and -2.31, respectively). The change in τ_{PC} reflects the reduction of primary emissions from plants and other anthropogenic sources as the result of regulations by air policies. Values of α_T decreased by -3.3 to - 30.5 % in Europe, North Africa, and the Middle East, which means the mean size of aerosol particles increased. Particle size on average became smaller over India and Asian regions considered in our study. We find that α_T increased by 1.3 to 13.1 %. In particular, α_{PF} increased in most areas., showing the probability that the average particle size of fine-mode aerosols became smaller in recent years.

Key words: aerosol optical depth, Ångström exponent, annual variation, fine-mode aerosol, AERONET

https://doi.org/10.5194/acp-2022-219
Preprint. Discussion started: 22 April 2022

Atmospheric Chemistry and Physics
Discussions

1. Introduction

Atmospheric aerosols are associated with air pollution and public health (Ramanathan et al., 2007; Ramanathan and Carmichael, 2008; Ipcc, 2019). In particular, small aerosol particles are damaging human health (WHO, 2016; Schraufnagel et al., 2019). The International Agency for Research on Cancer (IARC) classifies aerosol particles as a class 1 carcinogen (Loomis et al., 2013). The World Health Organization (WHO) is focusing on the number concentration of ultra-fine particles (WHO, 2021). Because of the hazard of particulate matter (PM), governments worldwide are continuously monitoring and controlling the mass concentration of PM (Collaud Coen et al., 2013; Li et al., 2014; Li et al., 2015; Mehta et al., 2018; Yang et al., 2018; Pozzer et al., 2019; Chirasophon and Pochanart, 2020; Liu et al., 2020). Particle size distribution however cannot be inferred from mass concentration observations (Lee et al., 2010; Burton et al., 2014). To understand the change in air pollution caused by PM and its adverse health effects, we need to identify the variations in size of small particles as well as mass concentration.

According to their sources, ambient atmospheric aerosols can be divided into natural and anthropogenic ones. Anthropogenic aerosols are emitted from industry activities, population growth, and combustion activities. Aerosols are also classified as fine- and coarse-mode particles depending on their size. Coarse-mode particles are related to primary emissions like industrial activities and biomass burning. This type of particle is highly correlated with the change of mass concentration (Han et al., 2015; Hatakeyama, 2017). Fine-mode particles are mainly considered as secondary aerosols formed by gaseous precursors, oxidants, and/or changes of meteorological conditions (Kitamori et al., 2009; Cheng and Li, 2010; Xue et al., 2014; Mesquita et al., 2016; Tan et al., 2017; Xu et al., 2017; Kong et al., 2018; Kudo et al., 2018; Wang et al., 2019). This particle type is closely related to visibility and adverse effects on human health. Liu et al., 2020 stated that secondary aerosols such as $PM_{2.5}$ still cause haze as the result of high pollution levels, despite the fact that aerosol mass concentration levels have decreased in Beijing in recent years.

Many studies show that aerosol mass concentration and aerosol optical depth (AOD, τ) have decreased globally in recent years (Li et al., 2014; Li et al., 2015; Mehta et al., 2018; Pozzer et al., 2019; Cherian and Quaas, 2020; Liu et al., 2020; Dehkhoda et al., 2020). However, these changes vary by region. These parameters provide little information on the optical properties and size distribution of the pollution particles. Plus, we have difficulty confirming the change of fine-mode particles using changes of mass concentration.

This research developed a method to separate τ as dust and coarse-/fine-mode pollution particles using size distribution and the linear depolarization ratio (δ_p). This method was applied to the long-term observation data of the Aerosol Robotic Network (AERONET) sun/sky radiometer (Dubovik et al., 2002; Omar et al., 2005; Levy et al., 2007; Mielonen et al., 2009; Lee et al., 2010; Russell et al., 2010) to determine aerosol types. We also analyzed the proportion of fine mode in the total aerosols, particle size characteristics change, and regional characteristics (Dubovik et al., 2002; Noh et al., 2011; Boselli et al., 2012).

https://doi.org/10.5194/acp-2022-219
Preprint. Discussion started: 22 April 2022

2. Methodology

2.1. Study sites

We selected AERONET Sun/sky radiometer sites that meet the following criteria: First, the sites have acquired data continuously for more than nine years since 2001, making them suitable for studying the long-term trend of τ. Second, the depolarization ratio is essential to calculate dust ratio, so we have limitations in using data in American and European sites. Third, the selected observation sites need to be representative of regional characteristics.

Eventually, we chose 17 AERONET sites to identify the annual change of regional aerosol particle characteristics. These sites are distributed across six regions, i.e., Europe, North Africa, Middle East, India, Southeast Asia, and Northeast Asia (Figure 1). The stations Venice (Italy, 45.310° N, 12.51° E), Thessaloniki (Greece, 40.63° N, 22.96° E) are located in Europe. We also add Erdemli (Turkey, Institute of Marin Science-Erdemli, 36.56° N, 34.26° E) to the European site as Turkey is bordering the eastern Mediterranean Sea.

There are four sites in Africa. Tamanrasset (Algeria, 22.79° N, 5.53° E) and the Cape Verde (16.73° N, 22.94° W) stations are located in the dust emission belt that stretches from North Africa westward out into the Atlantic Ocean. Cinzana (Mali, 13.28° N, 5.93° W) is located in the northwest part of the Sahel zone and is mainly affected by Saharan dust outbreaks. Ilorin (Nigeria, 8.48° N, 4.67° E) is located at the upper tip of the Guinea savannah zone in the sub-Sahel. This station is mainly influenced by Saharan dust and biomass burning aerosol (Balarabe et al., 2016).

There are two measurement sites in the Middle East. i.e., Sede Boker (Israel, 30.86° N,34.78° E) and Mezaira (the United Arab Emirates, 23.10° N, 53.75° E). The regions in India, i.e., Kanpur (26.51° N, 80.23° E) and Ballia (Gandhi_College, 25.87° N, 84.13° E) are in Uttar Pradesh which is a state in northern India. These sites are influenced mainly by large-scale anthropogenic emission sources (biomass burning, fossil-fuel combustion, and industrial activities) and mineral dust transported from western India (Ram et al., 2010).

Two Southeast Asia sites, Chiang Mai (18.77° N, 98.97° E) and Bangkok (Silpakorn University, 13.82° N, 100.04° E) are located in northern and central Thailand and have the characteristics of an urban environment. Four sites, Beijing (China, 39.98° N, 116.38° E), Seoul (Korea, 37.46° N, 126.95° E), Osaka (Japan, 34.65° N, 135.59° E), and Taipei (Taiwan, 25.02° N, 121.54° E) are representative regions in Northeast Asia. Beijing is known as the region with the highest concentration of pollution particles worldwide (Li et al., 2014). Seoul is downwind of westerly winds from Beijing and thus often affected by long-range transport of pollution particles from China. Seoul also has a high concentration of locally produced pollution particles. Osaka is a coastal city that produces less anthropogenic pollution than China and Korea. The effect of long-range transport of pollution on Taipei is relatively low.

Northeast Asia and Indian areas are the regions with high levels of aerosol emissions globally; so, we need to observe aerosol properties intensely. All 17 sites provide us with version 3 level 2.0 data for a minimum of 9 years. The total number of observation days per year is shown in Supplementary Table S1.

https://doi.org/10.5194/acp-2022-219
Preprint. Discussion started: 22 April 2022

2.2. AOD separation into dust, coarse- and fine-mode pollution using depolarization ratio

WHO recommended type classification of PM like black carbon or elemental carbon (BC/EC), ultrafine particles (UFP), and particles originating from sand and dust storms (SDS) to manage control of emission of aerosols effectively (WHO, 2021). Although not explicitly classified based on WHO guidelines, we divided aerosol types as dust, fine- and coarse-mode particles depending on depolarization ratio and particle size data.

Dubovik et al., 2006 introduced kernel look-up tables that describe mixtures of spheroid particles. These kernel look-up tables are used to infer the depolarization ratio (δ_p) of mineral dust observed with AERONET sun/sky radiometer. Details of the AERONET inversion algorithm are given by Dubovik et al., 2006 and Noh et al., 2017.

The dust ratio (R_D) was used to estimate the contributions of dust and anthropogenic pollution/biomass burning particles to the total aerosol optical depth ($\boldsymbol{\tau_T}$) of mixed aerosol plumes under the assumption that both types of aerosol particles are externally mixed (Shimizu et al., 2004; Tesche et al., 2009; Noh, 2014). R_D was retrieved from the linear particle depolarization ratio (δ_p). Noh et al., 2017 have shown that the δ_p derived from Sun/sky radiometer observations at 1020 nm and the lidar-derived δ_p at 532 nm show a comparably high correlation. For that reason, we used the δ_p at 1020 nm to retrieve the dust ratio (R_D). Shimizu et al., 2004 and Tesche et al., 2009 suggested a R_D retrieval method on the basis of

$$R_D = \frac{(\delta_p - \delta_2)(1+\delta_1)}{(\delta_1 - \delta_2)(1+\delta_p)} \quad (1)$$

The parameters δ_1 and δ_2 denote the δ_p at 1020 nm of pure dust and non-dust particles, respectively, of an external mixture of aerosol particles. The values δ_1 and δ_2 can be empirically determined. We use 0.31 for δ_1 in Europe, North Africa, the Middle East, and India. We use 0.30 for the Southeast and Northeast Asia regions, respectively. Those values were determined by the linear depolarization ratios of Saharan and Asian dust presented in previous research work (Freudenthaler et al., 2009; Burton et al., 2014; Shin et al., 2018). We used 0.02 as the minimum value for δ_2. When δ_p was higher than δ_1 or lower than δ_2, R_D was set to 1 or 0, respectively.

The coarse-mode fraction (CMF) of particles observed at 1020 nm is calculated from the ratio of the coarse-mode AOD to the total (coarse- and fine- mode) AOD. Thus, R_D represents the proportion of AOD for pure dust particles in a mixed aerosol plume, while CMF denotes the ratio of coarse-mode particles to the total particle AOD. Besides, the fine-mode fraction (FMF) is calculated as (1-CMF).

The correlation coefficient (R^2) of the linear regression between CMF and RD varies from 0.21 to 0.84 for the different observation sites (Figure S1, supplementary material). Chiang Mai, Bangkok, and the Taipei sites show low R^2 values of 0.34, 0.21, and 0.33, respectively. Since those sites are not located in the main transport route of Asian dust, the influence of dust particles is comparably weak compared to the other sites. The tendency for R_D to increase as CMF increases appears in all sites despite the weak correlation we find in our study.

Most of the dust particles are coarse-mode particles, which means that the value of CMF increases with R_D. CMF is higher than R_D in most cases, which implies that these coarse-mode particles include dust and pollution particles generated by physical and chemical reactions, e.g., coagulation, condensation processes, and hygroscopic growth (Noh et al., 2017). The ratio of coarse-mode particles (CMP) denotes the proportion (number concentration) of

https://doi.org/10.5194/acp-2022-219
Preprint. Discussion started: 22 April 2022

coarse-mode pollution particles to total particles. In here, dust particles are not considered. This ratio can be calculated by subtracting R_D from CMF at 1020 nm.

$$\mathrm{CMP}_{1020} = \mathrm{CMF}_{1020} - R_D \tag{2}$$

If R_D is higher than CMF, CMP is set to 0.

AOD of dust particles (τ_D) at 1020 nm was calculated with equation (3) and the use of R_D and S_d.

$$\tau_{D,1020} = \tau_{1020} \times R_D \times \frac{S_{d,1020}}{S_{1020}} \tag{3}$$

Here, 1020 denotes the wavelength at 1020 nm. The parameter S is the lidar ratio of the aerosol mixture. S can be calculated from the AERONET data products. The S_d is the lidar ratio of pure dust particles. It varies in dependence on the desert source. We take the value of 44 and 54 sr at 1020 nm for Asian dust and Saharan dust, respectively (Shin et al., 2018).

The AOD of coarse-mode particles (τ_{PC}) observed at 1020 nm was calculated by equation (4). τ_{PC} at 440, 675, and 870 nm was retrieved by equation (5), i.e.,

$$\tau_{PC,1020} = \tau_{1020}(\mathrm{CMP}) \tag{4}$$

$$\tau_{PC,\lambda} = \tau_{PC,1020}\left(\frac{1020}{\lambda}\right)^{\alpha_{PC}} \tag{5}$$

The term α_{PC} is the Ångström exponent of coarse-mode pollution. We used the value of 0.16 and 0.14 for Asian and Saharan dust, respectively (Shin et al., 2018).

We used equation (5) to calculate the AOD of the fine-mode pollution (τ_{PF}) contribution

$$\tau_{PF,\lambda} = \tau_\lambda - \tau_{D,\lambda} - \tau_{PC,\lambda} \tag{6}$$

2.3. Annual trend analysis via linear regression analysis and MK-test

To identify annual variation trends and regional properties, we calculated the change of τ with three methods. First, we used linear regression analysis on the time series of annual average τ, and we checked the slope and percent variation from 2001 to 2018. Second, we used the linear regression equation y=a+bx, where x is the time (year), and y is the annual average of τ. The slope b describes the change of τ; a is the intercept. The percent variation was calculated from the equation

$$V(\%) = \left(\frac{aN}{\bar{\tau}}\right) \times 100, \tag{7}$$

where $\bar{\tau}$ is the average of τ, N is the number of available data, and a is the slope obtained from the linear regression analysis. The p-value (probability value) is a scalar that describes how likely it is that the data occurred by random chance. The p-value should be small enough, depending on the level of confidence. We calculated all data and found a statistically significant trend.

We also applied the non-parametric Mann-Kendall (MK) statistical test (Mann, 1945; Kendall, 1975) and Sen's slope values to find annual trend and variation (Salmi et al., 2002; Srivastava and Saran, 2017). The MK-test provides reliable information on the significance of monotonic trends of data in a time series. The magnitude of the trend can be explained by Sen's slope test, which is a powerful method for investigating linear trends. There

https://doi.org/10.5194/acp-2022-219
Preprint. Discussion started: 22 April 2022

are two hypotheses on the MK-test. Hypotheses are decided by the significance of the value of Z, which is related to the p-value. The following relationships are used:

H_0 : null hypothesis (no trend),

H_1 : alternative hypothesis (clear trend),

$$\text{Critical value}: \; |Z| < 1.96 \; Accept\ H_0 \; (95\%\ Confidence\ level),$$
$$|Z| < 1.65 \; Accept\ H_0 \; (90\%\ Confidence\ level),$$
$$\text{otherwise}, \; |Z| > 1.96 \; Accept\ H_1 \; (95\%\ Confidence\ level),$$
$$|Z| > 1.65 \; Accept\ H_1 \; (90\%\ Confidence\ level).$$

The sign of Z indicates an increase (+) or decrease (-). The Z value is generally accepted at a 95 % confidence level, but the values and number of analysis elements are too small, so we used confidence levels up to 90% instead.

3. Results

3.1. Aerosol-type classification

In preparation for separating AOD according to dust-only and coarse- and fine-mode pollution AOD, we carried out an aerosol-type classification to understand the main aerosol types of each selected site. Shin et al., 2019 suggested a new aerosol type classification method. The authors proposed considering a) the contribution of mineral dust to the aerosol mixture based on a threshold value, denoted as R_D, which could be obtained from the depolarization ratio, in combination with b) the use of the single-scattering albedo (SSA). This latter parameter allows for identifying absorption properties of pollution/biomass burning aerosols and thus separating this aerosol type from mineral dust. In this study, we used seven aerosol types based on the values of δ_p, respectively. Aerosols were classified as pure dust (PD, R_D >0.89), dust-dominated mixture (DDM, 0.53≤ R_D ≤0.89), pollution-dominated mixture (PDM, 0.17≤ R_D <0.53), and pollution particles (R_D <0.17). Particles are classified on the basis of SSA as non-absorbing (NA, SSA>0.95), weakly-absorbing (WA, 0.90<SSA≤0.95), moderately absorbing (MA, 0.85≤SSA≤0.90), and strongly absorbing (SA, SSA<0.85) pollution; see Figure 3 of Shin et al., 2019.

Figure 2 shows the annual changes of major aerosol types at the 17 sites from 2001 to 2018. The results of our aerosol classification reflect the characteristics of the six regions well. In Europe, Southeast Asia, and Northeast Asia, pollution particles are the main type of aerosols. In the Middle East and North Africa, pure dust is dominant. The ratio of NA and WA is high but decreases in the order of Venice, Thessaloniki, and Erdemli. These regions have low values of PDM and DDM ratios, respectively. With regard to the North African region, the Sahara Desert obviously is the predominant source region. Naturally, PD is the predominant aerosol type. Ilorin in the Savannah region of Africa has a higher ratio of SA than other African regions as a result of biomass-burning aerosols. Sede Boker and Mezaira, which are located on the Arabian Peninsula, also show PD and DDM as the major aerosol types. The aerosol types of MA and WA can also be observed in Ilorin. The aerosol types MA and SA appear in

https://doi.org/10.5194/acp-2022-219
Preprint. Discussion started: 22 April 2022

Atmospheric Chemistry and Physics Discussions

Sede Boker and Mezaira but are not as dominant as dust. Thus, anthropogenic pollutants at Ilorin are higher than in the other African regions investigated in our study. Logothetis et al., 2020 reported that coarse-mode absorbing aerosols are dominant in North Africa and the Arabian Peninsula because of dust transported from the Saharan and the Arabian deserts. However, fine-mode particles emitted from human activity in the Arabian Peninsula are also observed in autumn and winter.

The ratio of dust and pollution particles at Kanpur and Ballia in northern India are similar. Chiang Mai and Bangkok, located in the Indochina Peninsular, are affected mainly by man-made pollution aerosols. The contribution from dust is comparably low. We find 5 % for PDM at most. However, these two regions have differences in that the predominant aerosol types over Chiang Mai and Bangkok are SA and WA, respectively. The high value of SA at Chiang Mai is due to biomass burning aerosols emitted by agricultural burning and forest clearing activities during the dry season which lasts from November to April (Janjai et al., 2012). Bangkok has a low average SSA value of 0.90, but the SA ratio is lower than that of Chiang Mai because the impact of biomass burning is lower (Bridhikitti and Overcamp, 2011).

The Northeast Asian region seems to be affected by both dust and pollution. Asian dust heavily affects the Northeast Asian region in spring, i.e., March, April, and May (Liu et al., 2019). The ratio of DDM and PDM is high in Beijing which is comparably close to the source regions of Asian dust. Seoul is located downwind of the emission regions. The impact of dust is relatively low in Osaka, which is relatively far from the source region. Besides, the Osaka site is not in the main transport pathway of dust. Shin et al., 2015 stated that dust might mix with pollution when the dust is transported near the surface for a long time. Taipei has the lowest dust effect because it is not located on the pathway of Asian dust.

3.2. Annual trend of dust, coarse- and fine-mode pollution AOD

One aim of our study is to learn more about how AOD may depend on aerosol particle size. Thus, we separated AOD into the contribution by dust-only (τ_{D}), coarse-mode pollution (τ_{PC}), and fine-mode pollution (τ_{PF}). We used R_{D}, CMF, and the relationships of equations (1) to (6). Then, we investigated the change of annual mean values and the regional differences.

Before separating AODs according to aerosol types, we compared trends in the average values of τ_{T} for each region and site during 2001–2018 (supplementary Figure S2). The average value of τ_{T} at 440 nm was highest (1.22 ± 0.76) in Beijing and was lowest (0.48 ± 0.12) in Thessaloniki. Regionally, Northeast Asia (1.22–0.58), Southeast Asia (0.93–0.76), and India (0.82–0.80) show high τ_{T} values. Europe (0.54–0.48) and the Middle East (0.56–0.49) show low values. The average τ_{T} value of North Africa except Ilorin (1.04 ± 0.48) tends to be at the lower end of values (Table 1).

The remarkable thing is the change of the annual averages of τ_{T}. This change is summarized for each site in Table 2. Values of τ_{T} decreased every year in Northeast Asia and Europe. Notably, Beijing showed the most prominent decreasing trend of τ_{T}. We find an average value of -0.0138 $\tau_{\mathrm{T}} yr^{-1}$. The Chiang Mai and Bangkok sites in Southeast Asia showed a decrease of τ_{T}, too. We find average values of -0.0039 $\tau_{\mathrm{T}} yr^{-1}$ and 0.0012 $\tau_{\mathrm{T}} yr^{-1}$

https://doi.org/10.5194/acp-2022-219
Preprint. Discussion started: 22 April 2022

at these two sites, respectively. However, this decrease of τ_T showed considerable change depending on the years considered in our study. We find, for example, that τ_T was slightly higher from 2008 to 2016 (0.00117 $\tau_T yr^{-1}$ for Chiang Mai and 0.0107 $\tau_T yr^{-1}$ for Bangkok) and then sharply decreased in 2017 (Figure S2(e)).

The Middle East, India, and North Africa except Cinzana showed an increase of τ_T with time. As shown in Table 2, the rate of annual change of τ_T at Ballia and Kanpur showed a clear tendency to increase. We find 0.0048 $\tau_T yr^{-1}$ and 0.0069 $\tau_T yr^{-1}$, respectively. In most North Africa and the Middle East regions, the change rate of τ_T (-0.006 to 0.0020 $\tau_T yr^{-1}$) is lower than other regions; however, τ_T of Tamanrasset sites increased as 0.0108 $\tau_T yr^{-1}$ because of τ_D. It is supported by the results from El-Metwally et al., 2020. The authors conclude that Tamanrasset is the site most affected by dust from the downwind Saharan sources in the Saharan/Arabian region.

Other studies also confirmed this trend of regional τ_T change. Balarabe et al., 2016 reported that, based on AERONET data, there were no remarkable AOD trends for the period from 1998 to 2013 over Ilorin, Nigeria. Maghrabi and Alotaibi, 2018 reported a significant increase of approximately 0.119 of the annual mean AOD at 500 nm measured by AERONET sunphotometer in the central Arabian Peninsula from 1999 to 2015. Klingmüller et al., 2016 also stated that AOD increased in Saudi Arabia between 2001 and 2012. (Pilahome et al., 2020) reported an increase of AOD at 550 nm across Thailand based on analyzing MODIS (Moderate Resolution Imaging Spectroradiometer) data for the years 2006 to 2016. In addition, the change in the concentration of particulate matter, expressed by AOD, was attributed to different aerosol types. The authors identified the following aerosol types in decreasing order of importance: biomass burning, anthropogenic pollution, and soil emission. Meteorological conditions played a significant role, too (Bridhikitti and Overcamp, 2011; Wang et al., 2015; Yin et al., 2019; Chirasophon and Pochanart, 2020).

The annual mean of dust-only AOD (τ_D) was high in North Africa, naturally, because dust is a major aerosol type in that part of the world. We find low values of τ_D in Southeast Asia, see Figure 2. In the India and Northeast Asia region except for Beijing, the annual change of τ_D tended to decrease from -0.004 to -0.002 $\tau_D yr^{-1}$ (Table 2). In case of Beijing, τ_D increased by 36.3% (0.0011 $\tau_D yr^{-1}$). In Europe, Middle East Asia, and North Africa, the annual rate of change increased from 0.002 to 0.0133 $\tau_D yr^{-1}$. The exception is Ilorin, where we find -0.3% (-0.0001 $\tau_D yr^{-1}$).

We assume that non-dust AOD values describe anthropogenic emissions and local biomass burning. Anthropogenic emissions mainly belong to the fine-mode fraction of the particle size distribution; therefore, denote their contribution to AOD as τ_{PF}. In contrast, locally emitted particles from biomass burning belong to the coarse-mode fraction of pollution. We denote this part of AOD as τ_{PC}.

The annual average values of τ_{PC} slightly increased in Europe, North Africa, and India, and decreased in the Middle East and Northeast Asia. We find values between -0.0015 and 0.0004 $\tau_{PC} yr^{-1}$. These numbers show that we need to consider percent variations to compare the rate of change by region, because the rate of change depends on the initial value. Especially, it is difficult to confirm the evident change of τ_{PC} in Europe and India. The percent variation in Thessaloniki and Ballia was 11.9% and 10.5%, respectively.

https://doi.org/10.5194/acp-2022-219
Preprint. Discussion started: 22 April 2022

Atmospheric Chemistry and Physics
Discussions

The annual average value of τ_{PF} also varied by region. The mean changes of τ_{PF} (at 440 nm) for the observation site in India show a clear tendency towards increasing values. We find 0.0055 $\tau_{PF} yr^{-1}$ for Ballia and 0.0019 $\tau_{PF} yr^{-1}$ for Kanpur. In the other regions, except for Erdemli (Europe), Ilorin, Tamanrasset (North Africa), and Sede Boker (Middle East), the changes of mean τ_{PF} tended to decrease significantly compared to τ_D and τ_{PC}. We find values between -0.0011 to -0.0142 $\tau_{PF} yr^{-1}$. The stations at Erdemli, Ilorin, Tamanrasset, and Sede Boker showed a slight increase of τ_{PF}, i.e., 0.0005, 0.0024, 0.0001, and 0.0008 $\tau_{PF} yr^{-1}$, respectively.

In the next step, we analyzed changes of τ (increase and decrease) in terms of aerosol types. We used in our analysis the percent variation of τ_T, τ_D, τ_{PC}, and τ_{PF} (see Equation 7), respectively. We find a decline of τ_T and τ_{PF} in Europe. We find comparably high confidence levels of 95% (based on MK-test) for the stations in Thessaloniki and Venice, see Table 3. In addition, the slope of τ_D in Thessaloniki and Venice (using the linear-regression method) was 0.0037 $\tau_D yr^{-1}$ and 0.0012 $\tau_D yr^{-1}$, but the percent variation was as high as 112.29% (Thessaloniki) and 125.22% (Venice).

τ_T decreased for the Asian stations, in a similar fashion to the sites in Europe. However, this change of τ_T was different for the Southeast and Northeast Asian stations if we take account of the aerosol types.

With respect to Southeast Asia, the decrease of τ_T seems to be mainly caused by a decrease in emissions of fine-mode particles. In Northeast Asia, changes in τ showed different characteristics according to region. The MK-test shows 95% confidence level for the trends observed for τ_T (Beijing and Osaka), τ_D (Osaka), τ_{PC} (Seoul and Osaka), and τ_{PF} (Beijing and Osaka).

Non-dust coarse-mode particles are mainly emitted from sources related to anthropogenic activities, e.g., traffic and plants. Regulations on emissions of air pollution thus may be responsible for the lower concentrations of this type of coarse-mode particles (Bridhikitti and Overcamp, 2011; Mehta et al., 2018).

In the case of Beijing, which is affected by high levels of air pollution, τ_D increased by 36.2% (0.0011 $\tau_D yr^{-1}$). The non-dust part of AOD, and particularly the AOD related to fine-mode particles (τ_{PF}), seemed to decrease by -38.1% (-0.0142 $\tau_{PF} yr^{-1}$). Thus, taking account of all three components, we find that the decrease of fine-mode pollution mainly causes a decrease in total AOD. This result is similar to results reported in previous research (Li et al., 2015). The authors show that black carbon in China decreased due to the strict policy of reduction of pollution emissions. Li et al. (2015) furthermore stated that dust aerosol concentrations had increased between 2002 and 2006 but then remained constant between 2008 and 2013.

The annual change of τ_T for the stations in North Africa increased during (0.0006–0.0108 $\tau_D yr^{-1}$) over ten more years. The exception is the station at Cinzana. The properties of the variations seem to be different for the different regions. The percent variation of the $\tau_T$increase at Tamanrasset is quite obviously related to a change of τ_D. The Cape Verde and Ilorin stations showed a slightly increasing trend, most likely caused by a change of coarse- and fine-mode particles. Cinzana is the only site of all North African stations where we find a decrease of τ_T. This decrease seems to be driven by a decrease in τ_{PF}.

The τ_D in the Middle East increased, which resulted in an increase of total optical depth. In the case of India, the change of τ_T is related to a decrease in τ_D and an increase in τ_{PC} and τ_{PF}. The increase in τ_{PC} and τ_{PF} may

https://doi.org/10.5194/acp-2022-219
Preprint. Discussion started: 22 April 2022

be associated with new policies related to aerosol emissions in the Indian regions considered in this study (Khan et al., 2019; Yin et al., 2019).

A comprehensive graph of the annual average, the overall increase, and the percent variation associated with total, dust-only, and coarse- and fine-mode pollution AOD is presented in Figure 3.

3.2. Ångström Exponent and FMF: Annual Trends

Our analysis shows regional differences in aerosol type and size changes which can be inferred from annual mean values of AOD, see Table 2. In addition to this result, we examined the change of particle size distribution, especially that of fine-mode particles, more closely by using the Ångström exponent of total (α_T) and fine-mode particles (α_{PF}) and the FMF (fine-mode fraction). The changes of α_T and α_{PF} also can be seen in supplementary Figures S6 and S7. The value of α_{PF} indicates the presence of anthropogenic pollution particles. FMF describes the fraction of fine-mode particles compared to all particles in the atmospheric column observed by the sun photometer (Table 2). Figure 4 shows the comprehensive results of the average value, the increasing rate, and the percent variation of α_T and α_{PF}.

The α_T in Europe, North Africa, and the Middle East regions except Ilorin decreased during the research period we analyzed. We find negative values ranging from -3.3% to -30.5%. FMF decreased by -3.7% to -21.1%. These trends show that the particles on average became larger. This result is similar to the main findings discussed in the previous section, where we showed that τ_D and τ_{PC} increased and τ_{PF} decreased. These changes are associated with increased levels of dust particle concentration and reduced levels of fine-mode particles due to climate change (Bridhikitti and Overcamp, 2011; Krasnov et al., 2014; Klingmüller et al., 2016) and environmental regulations (Li et al., 2015; Mehta et al., 2018; Pozzer et al., 2019; Chirasophon and Pochanart, 2020). The Ilorin site in Nigeria is different from the other North African regions. Ilorin is located in the transition zone between the humid tropical area (South Africa) and the semi-arid area (North Africa) (Ogunjobi et al., 2008; Falaiye et al., 2015). This site also exhibits an increase in anthropogenic emissions caused by the rapid increase of population and economic growth (Balarabe et al., 2016).

Additionally, we checked if changes of α_{PF} corroborate our assumption that characteristics of the size distribution of the fine-mode particles also changed. The values of α_{PF} in Europe, North Africa, and the Middle East except Erdemli (Turkey) and Mezaira (UAE) show positive trends, i.e., 0.0015 yr^{-1} to 0.0101 yr^{-1}. These increases indicate that the size of the fine-mode particles became smaller.

The annual mean of α_T at Ballia and Kanpur increased in 0.0050 yr^{-1} (4.9%) and 0.0024 yr^{-1} (4.1%), respectively. These increases indicate that particle size became smaller. The increase of the FMF value corroborates this result. The values of α_{PF} showed a positive trend at the Kanpur site, which means that fine-mode particles became smaller over the course of several years. The negative values of α_{PF} in Ballia might be caused by the comparably few data points available for the first few years of observations (Supplementary Table S1). Kanpur is a highly polluted city in the Indo-Gangetic region (Chakraborty et al., 2015; Chen et al., 2016) which may explain in large part the high concentration of small particles in this region.

In Southeast Asia, the values of α_T increased. We find 0.0105 yr^{-1} (6.7%) at Chiang Mai and 0.0119 yr^{-1} (8.0%) in Bangkok. α_{PF} showed a more increasing trend compared to α_T as 0.0163 yr^{-1} (9.0%) and 0.0175 yr^{-1} (10.0%) at Chiang Mai and Bangkok, respectively. On the contrary, FMF showed a negative trend as -0.0022 (-0.9%) at Ching Mai and -0.0002 (-0.1%) at Bangkok. Considering that the major aerosols in Southeast Asia are biomass burning aerosol and anthropogenic aerosol composed of fine-mode aerosol, it is estimated that the particle size of these two types is continuously decreasing (Chirasophon et al., 2020; Bridhikitti et al., 2011; Khan et al., 2019; Yin et al., 2019).

The values of α_T in Northeast Asia have a bit of difference to 1.3–13.3% depending on stations. For example, Seoul and Taipei had highly positive increases of α_T. That positive increases could be related to reducing the dust concentration, which would lead to a significant decrease of τ_{PC} compared to that of τ_{PF}. For Beijing, the α_T slightly increased compared to the other sites. Our data show that τ_D increased. In addition, the decrease of τ_{PC} was more significant than the decrease of τ_{PF}. Thus, we come to the conclusion that the increase of α_T most likely was caused by a change in the atmosphere's dust load.

The α_{PF} values in the Asian region increased by 2.3% to 13.1 % (0.0024 to 0.0175 yr^{-1}) over the observation periods considered in our study. The data indicate that fine-mode particle size became smaller over the years and that this change might also be related to changes in the chemical composition of the pollution particles. Joo et al., 2021 reported that extinction efficiencies in Korea increased although the $PM_{2.5}$ mass concentration decreased. This result suggests that even though the $PM_{2.5}$ concentration decreased compared to the past, either particle size of $PM_{2.5}$ became smaller or the number of particles with high scattering efficiency increased. Uno et al., 2020 stated that the chemical composition of aerosols in East Asia changed significantly. With regard to regions downwind of China, sulfate (accumulation mode) concentrations decreased significantly, and nitrate (accumulation–coarse mode) concentrations increased (Plaza et al., 2011). These results show that there clearly is a need to conduct more long-term studies on the relationship between aerosol mass and optical density, size distribution, and chemical composition.

4. Summary and Conclusion

We analyzed trends in regional AOD based on separating aerosols into dust and coarse- and fine-mode pollution particles for 17 AERONET observation sites. Mainly, we focused on the change in AOD and Ångström exponents of fine-mode pollution particles (τ_{PF} and α_{PF}). The following key results were obtained:

- The change characteristics of τ_D, τ_{PC}, and τ_{PF} are different for each region. In Europe and Asia, the decrease in τ_T was remarkable due to effects caused by new air policies. The τ_D increased near the Sahara region.
- The τ_{PF} mainly decreased in Europe and Southeast Asia, whereas τ_{PC} decreased in the Middle East and Northeast Asia. τ_{PC} and τ_{PF} are related to non-dust AOD. Thus, we assume that changes related to the practical policymaking have on air pollution emissions.

- The mean size of particle size distribution became larger in Europe, the Middle East, and North Africa because of emissions of dust particles. On the other hand, the mean particle size became smaller in India and Southeast Asia. We assume that this reduction of particle size is primarily related to the change in the concentration of fine-mode particles.
- The changes of α_{PF} show that the size of fine-mode particles emitted from anthropogenic pollution most likely became smaller compared to particle size in past times in the regions we investigated here. We believed that the size change of fine-mode particles might be related to secondary aerosols, and it can cause adverse effects on visibility and human health.

Particle size and characteristics are essential to understanding air pollution and visibility and have changed over the past decade or more, but few studies about those properties. Therefore, we need more studies paying attention to changes in the size and quantity of fine-mode pollution particles to reflect air pollution policy.

Author contributions

JS1(J.Shin) and JS2(J.sim) analyzed data; ND, SJ, TK, GK collected resources; SS and DS advised the methodology and curated data; YN supervised all the research; JS1 wrote the manuscript draft; DM, MT, and YN wrote review and editing;

Acknowledgement

This work was supported by the National Research Foundation of Korea (NRF). Funding was provided by the Ministry of Science and ICT (MSIT) and the Ministry of Education (MOE), Republic of Korea (grant No. 2019M3E7A1113103).
We thank the PIs of the AERONET group for providing their data to the community. We would also like to thank AERONET for their efforts in offering high-quality data and derivative products. All data used in this are in the AERONET homepage at https://aeronet.gsfc.nasa.gov/

https://doi.org/10.5194/acp-2022-219
Preprint. Discussion started: 22 April 2022

References

Balarabe, M., Abdullah, K., and Nawawi, M.: Seasonal Variations of Aerosol Optical Properties and Identification of Different Aerosol Types Based on AERONET Data over Sub-Sahara West-Africa, Atmospheric and Climate Sciences, 06, 13-28, 10.4236/acs.2016.61002, 2016.

Boselli, A., Caggiano, R., Cornacchia, C., Madonna, F., Mona, L., Macchiato, M., Pappalardo, G., and Trippetta, S.: Multi year sun-photometer measurements for aerosol characterization in a Central Mediterranean site, Atmospheric Research, 104, 98-110, 2012.

Bridhikitti, A. and Overcamp, T. J.: Optical characteristics of southeast Asia's regional aerosols and their sources, Journal of the Air & Waste Management Association, 61, 747-754, 2011.

Burton, S., Vaughan, M., Ferrare, R., and Hostetler, C.: Separating mixtures of aerosol types in airborne High Spectral Resolution Lidar data, Atmospheric Measurement Techniques, 7, 419-436, 2014.

Chakraborty, A., Bhattu, D., Gupta, T., Tripathi, S. N., and Canagaratna, M. R.: Real-time measurements of ambient aerosols in a polluted Indian city: Sources, characteristics, and processing of organic aerosols during foggy and nonfoggy periods, Journal of Geophysical Research: Atmospheres, 120, 9006-9019, 10.1002/2015jd023419, 2015.

Chen, H., Cheng, T., Gu, X., Li, Z., and Wu, Y.: Characteristics of aerosols over Beijing and Kanpur derived from the AERONET dataset, Atmospheric Pollution Research, 7, 162-169, 10.1016/j.apr.2015.08.008, 2016.

Cheng, Y.-H. and Li, Y.-S.: Influences of Traffic Emissions and Meteorological Conditions on Ambient PM10 and PM2.5 Levels at a Highway Toll Station, Aerosol and Air Quality Research, 10, 456-462, 10.4209/aaqr.2010.04.0025, 2010.

Cherian, R. and Quaas, J.: Trends in AOD, Clouds, and Cloud Radiative Effects in Satellite Data and CMIP5 and CMIP6 Model Simulations Over Aerosol Source Regions, Geophysical Research Letters, 47, 10.1029/2020gl087132, 2020.

Chirasophon, S. and Pochanart, P.: The Long-term Characteristics of PM10 and PM2.5 in Bangkok, Thailand, Asian Journal of Atmospheric Environment, 14, 73-83, 10.5572/ajae.2020.14.1.073, 2020.

Collaud Coen, M., Andrews, E., Asmi, A., Baltensperger, U., Bukowiecki, N., Day, D., Fiebig, M., Fjaeraa, A. M., Flentje, H., Hyvärinen, A., Jefferson, A., Jennings, S. G., Kouvarakis, G., Lihavainen, H., Lund Myhre, C., Malm, W. C., Mihapopoulos, N., Molenar, J. V., O'Dowd, C., Ogren, J. A., Schichtel, B. A., Sheridan, P., Virkkula, A., Weingartner, E., Weller, R., and Laj, P.: Aerosol decadal trends – Part 1: In-situ optical measurements at GAW and IMPROVE stations, Atmospheric Chemistry and Physics, 13, 869-894, 10.5194/acp-13-869-2013, 2013.

Dehkhoda, N., Noh, Y., and Joo, S.: Long-Term Variation of Black Carbon Absorption Aerosol Optical Depth from AERONET Data over East Asia, Remote Sensing, 12, 3551, 2020.

Dubovik, O., Holben, B., Lapyonok, T., Sinyuk, A., Mishchenko, M., Yang, P., and Slutsker, I.: Non-spherical aerosol retrieval method employing light scattering by spheroids, Geophysical Research Letters, 29, 54-51-54-54, 2002.

Dubovik, O., Sinyuk, A., Lapyonok, T., Holben, B. N., Mishchenko, M., Yang, P., Eck, T. F., Volten, H., Munoz, O., and Veihelmann, B.: Application of spheroid models to account for aerosol particle nonsphericity in remote sensing of desert dust, Journal of Geophysical Research: Atmospheres, 111, 2006.

El-Metwally, M., Korany, M., Boraiy, M., Ebada, E., Wahab, M. A., Hungershoefer, K., and Alfaro, S.: Evidence of anthropization of aerosols in the Saharan and peri-Saharan regions: Implications for the atmospheric transfer of solar radiation, Journal of Atmospheric and Solar-Terrestrial Physics, 199, 105199, 2020.

Falaiye, A., Babatunde, E., and Willoughby, A.: Atmospheric aerosol loading at Ilorin, a tropical station, The African Review of Physics, 9, 2015.

Freudenthaler, V., Esselborn, M., Wiegner, M., Heese, B., Tesche, M., Ansmann, A., Müller, D., Althausen, D., Wirth, M., and Fix, A.: Depolarization ratio profiling at several wavelengths in pure

https://doi.org/10.5194/acp-2022-219
Preprint. Discussion started: 22 April 2022

Saharan dust during SAMUM 2006, Tellus B: Chemical and Physical Meteorology, 61, 165-179, 2009.

Han, T., Xu, W., Chen, C., Liu, X., Wang, Q., Li, J., Zhao, X., Du, W., Wang, Z., and Sun, Y.: Chemical apportionment of aerosol optical properties during the Asia-Pacific Economic Cooperation summit in Beijing, China, Journal of Geophysical Research: Atmospheres, 120, 12,281-212,295, 2015.

Hatakeyama, S.: Aerosols, in: Air Pollution Impacts on Plants in East Asia, Springer, 21-42, 2017.

IPCC: Climate Change and Land: an IPCC special report on climate change, desertification, land degradation, sustainable land management, food security, and greenhouse gas fluxes in terrestrial ecosystems, 2019.

Janjai, S., Nunez, M., Masiri, I., Wattan, R., Buntoung, S., Jantarach, T., and Promsen, W.: Aerosol optical properties at four sites in Thailand, Atmospheric and Climate Sciences, 2, 441, 2012.

Joo, S., Naghmeh, D., and Noh, Y.: A Study on the Characteristic Variations of Fine Particle in Busan and Ulsan through Particle Extinction Efficiency Analysis, Journal of Korean Society for Atmospheric Environment, 37, 80-90, 10.5572/kosae.2021.37.1.080, 2021.

Kendall, M.: Rank Correlation Methods, Charles Griffin, London (1975), Google Sch, 1975.

Khan, R., Kumar, K. R., and Zhao, T.: The climatology of aerosol optical thickness and radiative effects in Southeast Asia from 18-years of ground-based observations, Environmental Pollution, 254, 113025, 2019.

Kitamori, Y., Mochida, M., and Kawamura, K.: Assessment of the aerosol water content in urban atmospheric particles by the hygroscopic growth measurements in Sapporo, Japan, Atmospheric Environment, 43, 3416-3423, 10.1016/j.atmosenv.2009.03.037, 2009.

Klingmüller, K., Pozzer, A., Metzger, S., Stenchikov, G. L., and Lelieveld, J.: Aerosol optical depth trend over the Middle East, Atmospheric Chemistry and Physics, 16, 5063-5073, 10.5194/acp-16-5063-2016, 2016.

Kong, L., Du, C., Zhanzakova, A., Cheng, T., Yang, X., Wang, L., Fu, H., Chen, J., and Zhang, S.: Trends in heterogeneous aqueous reaction in continuous haze episodes in suburban Shanghai: An in-depth case study, Sci Total Environ, 634, 1192-1204, 10.1016/j.scitotenv.2018.04.086, 2018.

Krasnov, H., Katra, I., Koutrakis, P., and Friger, M. D.: Contribution of dust storms to PM10 levels in an urban arid environment, Journal of the Air & Waste Management Association, 64, 89-94, 2014.

Kudo, S., Iijima, A., Kumagai, K., Tago, H., and Ichijo, M.: An exhaustive classification for the seasonal variation of organic peaks in the atmospheric fine particles obtained by a gas chromatography/mass spectrometry, Environmental Technology & Innovation, 12, 14-26, 2018.

Lee, K.-H., Muller, D., Noh, Y.-M., Shin, S.-K., and Shin, D.-H.: Depolarization ratio retrievals using AERONET sun photometer data, Journal of the Optical Society of Korea, 14, 178-184, 2010.

Levy, R. C., Remer, L. A., and Dubovik, O.: Global aerosol optical properties and application to Moderate Resolution Imaging Spectroradiometer aerosol retrieval over land, Journal of Geophysical Research: Atmospheres, 112, 2007.

Li, J., Carlson, B. E., Dubovik, O., and Lacis, A. A.: Recent trends in aerosol optical properties derived from AERONET measurements, Atmospheric Chemistry and Physics, 14, 12271-12289, 10.5194/acp-14-12271-2014, 2014.

Li, Z., Li, L., Zhang, F., Li, D., Xie, Y., and Xu, H.: Comparison of aerosol properties over Beijing and Kanpur: Optical, physical properties and aerosol component composition retrieved from 12 years ground-based Sun-sky radiometer remote sensing data, Journal of Geophysical Research: Atmospheres, 120, 1520-1535, 10.1002/2014jd022593, 2015.

Liu, D., Zhao, T., Boiyo, R., Chen, S., Lu, Z., Wu, Y., and Zhao, Y.: Vertical Structures of Dust Aerosols over East Asia Based on CALIPSO Retrievals, Remote Sensing, 11, 10.3390/rs11060701, 2019.

Liu, J., Ren, C., Huang, X., Nie, W., Wang, J., Sun, P., Chi, X., and Ding, A.: Increased Aerosol Extinction Efficiency Hinders Visibility Improvement in Eastern China, Geophysical Research Letters, 47, 10.1029/2020gl090167, 2020.

Logothetis, S.-A., Salamalikis, V., and Kazantzidis, A.: Aerosol classification in Europe, Middle East, North Africa and Arabian Peninsula based on AERONET Version 3, Atmospheric Research, 239, 10.1016/j.atmosres.2020.104893, 2020.

Loomis, D., Grosse, Y., Lauby-Secretan, B., Ghissassi, F. E., Bouvard, V., Benbrahim-Tallaa, L., Guha,

N., Baan, R., Mattock, H., and Straif, K.: The carcinogenicity of outdoor air pollution, The Lancet Oncology, 14, 1262-1263, 10.1016/s1470-2045(13)70487-x, 2013.
Maghrabi, A. and Alotaibi, R.: Long-term variations of AOD from an AERONET station in the central Arabian Peninsula, Theoretical and Applied Climatology, 134, 1015-1026, 2018.
Mann, H. B.: Nonparametric tests against trend, Econometrica: Journal of the econometric society, 245-259, 1945.
Mehta, M., Singh, N., and Anshumali: Global trends of columnar and vertically distributed properties of aerosols with emphasis on dust, polluted dust and smoke - inferences from 10-year long CALIOP observations, Remote Sensing of Environment, 208, 120-132, 10.1016/j.rse.2018.02.017, 2018.
Mesquita, S. R., Dachs, J., van Drooge, B. L., Castro-Jimenez, J., Navarro-Martin, L., Barata, C., Vieira, N., Guimaraes, L., and Pina, B.: Toxicity assessment of atmospheric particulate matter in the Mediterranean and Black Seas open waters, Sci Total Environ, 545-546, 163-170, 10.1016/j.scitotenv.2015.12.055, 2016.
Mielonen, T., Arola, A., Komppula, M., Kukkonen, J., Koskinen, J., De Leeuw, G., and Lehtinen, K.: Comparison of CALIOP level 2 aerosol subtypes to aerosol types derived from AERONET inversion data, Geophysical Research Letters, 36, 2009.
Noh, Y., Müller, D., Lee, K., Kim, K., Lee, K., Shimizu, A., Sano, I., and Park, C. B.: Depolarization ratios retrieved by AERONET sun–sky radiometer data and comparison to depolarization ratios measured with lidar, Atmospheric Chemistry and Physics, 17, 6271-6290, 2017.
Noh, Y. M.: Single-scattering albedo profiling of mixed Asian dust plumes with multiwavelength Raman lidar, Atmospheric Environment, 95, 305-317, 2014.
Noh, Y. M., Müller, D., Mattis, I., Lee, H., and Kim, Y. J.: Vertically resolved light-absorption characteristics and the influence of relative humidity on particle properties: Multiwavelength Raman lidar observations of East Asian aerosol types over Korea, Journal of Geophysical Research: Atmospheres, 116, 2011.
Ogunjobi, K. O., He, Z., and Simmer, C.: Spectral aerosol optical properties from AERONET Sun-photometric measurements over West Africa, Atmospheric Research, 88, 89-107, 10.1016/j.atmosres.2007.10.004, 2008.
Omar, A. H., Won, J. G., Winker, D. M., Yoon, S. C., Dubovik, O., and McCormick, M. P.: Development of global aerosol models using cluster analysis of Aerosol Robotic Network (AERONET) measurements, Journal of Geophysical Research: Atmospheres, 110, 2005.
Pilahome, O., Homchampa, C., and Kumharn, W.: Trends of Climate Variables and Aerosol optical Depth in Thailand, IOP Conference Series: Earth and Environmental Science, 012029,
Plaza, J., Pujadas, M., Gómez-Moreno, F., Sánchez, M., and Artíñano, B.: Mass size distributions of soluble sulfate, nitrate and ammonium in the Madrid urban aerosol, Atmospheric environment, 45, 4966-4976, 2011.
Pozzer, A., Bacer, S., Sappadina, S. D. Z., Predicatori, F., and Caleffi, A.: Long-term concentrations of fine particulate matter and impact on human health in Verona, Italy, Atmospheric Pollution Research, 10, 731-738, 10.1016/j.apr.2018.11.012, 2019.
Ram, K., Sarin, M., and Tripathi, S.: A 1 year record of carbonaceous aerosols from an urban site in the Indo-Gangetic Plain: Characterization, sources, and temporal variability, Journal of Geophysical Research: Atmospheres, 115, 2010.
Ramanathan, V. and Carmichael, G.: Global and regional climate changes due to black carbon, Nature Geoscience, 1, 221-227, 2008.
Ramanathan, V., Ramana, M. V., Roberts, G., Kim, D., Corrigan, C., Chung, C., and Winker, D.: Warming trends in Asia amplified by brown cloud solar absorption, Nature, 448, 575-578, 10.1038/nature06019, 2007.
Russell, P., Bergstrom, R., Shinozuka, Y., Clarke, A., DeCarlo, P., Jimenez, J., Livingston, J., Redemann, J., Dubovik, O., and Strawa, A.: Absorption Angstrom Exponent in AERONET and related data as an indicator of aerosol composition, Atmospheric Chemistry and Physics, 10, 1155-1169, 2010.
Salmi, T., Määttä, A., Anttila, P., Ruoho-Airola, T., and Amnell, T.: Detecting trends of annual values

https://doi.org/10.5194/acp-2022-219
Preprint. Discussion started: 22 April 2022

Atmospheric Chemistry and Physics Discussions

of atmospheric pollutants by the Mann-Kendall test and Sen's slope estimates MAKESENS–The excel template application, Finish Meteorological Institute, Helsinki, 2002.

Schraufnagel, D. E., Balmes, J. R., Cowl, C. T., De Matteis, S., Jung, S. H., Mortimer, K., Perez-Padilla, R., Rice, M. B., Riojas-Rodriguez, H., Sood, A., Thurston, G. D., To, T., Vanker, A., and Wuebbles, D. J.: Air Pollution and Noncommunicable Diseases: A Review by the Forum of International Respiratory Societies' Environmental Committee, Part 1: The Damaging Effects of Air Pollution, Chest, 155, 409-416, 10.1016/j.chest.2018.10.042, 2019.

Shimizu, A., Sugimoto, N., Matsui, I., Arao, K., Uno, I., Murayama, T., Kagawa, N., Aoki, K., Uchiyama, A., and Yamazaki, A.: Continuous observations of Asian dust and other aerosols by polarization lidars in China and Japan during ACE-Asia, Journal of Geophysical Research: Atmospheres, 109, 2004.

Shin, S.-K., Tesche, M., Noh, Y., and Müller, D.: Aerosol-type classification based on AERONET version 3 inversion products, Atmospheric Measurement Techniques, 12, 3789-3803, 2019.

Shin, S.-K., Müller, D., Lee, C., Lee, K., Shin, D., Kim, Y., and Noh, Y.: Vertical variation of optical properties of mixed Asian dust/pollution plumes according to pathway of air mass transport over East Asia, Atmospheric Chemistry and Physics, 15, 6707-6720, 2015.

Shin, S.-K., Tesche, M., Kim, K., Kezoudi, M., Tatarov, B., Müller, D., and Noh, Y.: On the spectral depolarisation and lidar ratio of mineral dust provided in the AERONET version 3 inversion product, Atmospheric Chemistry and Physics, 18, 12735-12746, 2018.

Srivastava, A. and Saran, S.: Comprehensive study on AOD trends over the Indian subcontinent: a statistical approach, International Journal of Remote Sensing, 38, 5127-5149, 10.1080/01431161.2017.1323284, 2017.

Tan, H., Cai, M., Fan, Q., Liu, L., Li, F., Chan, P. W., Deng, X., and Wu, D.: An analysis of aerosol liquid water content and related impact factors in Pearl River Delta, Sci Total Environ, 579, 1822-1830, 10.1016/j.scitotenv.2016.11.167, 2017.

Tesche, M., Ansmann, A., Müller, D., Althausen, D., Engelmann, R., Freudenthaler, V., and Groß, S.: Vertically resolved separation of dust and smoke over Cape Verde using multiwavelength Raman and polarization lidars during Saharan Mineral Dust Experiment 2008, Journal of Geophysical Research: Atmospheres, 114, 2009.

Uno, I., Wang, Z., Itahashi, S., Yumimoto, K., Yamamura, Y., Yoshino, A., Takami, A., Hayasaki, M., and Kim, B.-G.: Paradigm shift in aerosol chemical composition over regions downwind of China, Scientific reports, 10, 1-11, 2020.

Wang, H., Ding, J., Xu, J., Wen, J., Han, J., Wang, K., Shi, G., Feng, Y., Ivey, C. E., Wang, Y., Nenes, A., Zhao, Q., and Russell, A. G.: Aerosols in an arid environment: The role of aerosol water content, particulate acidity, precursors, and relative humidity on secondary inorganic aerosols, Sci Total Environ, 646, 564-572, 10.1016/j.scitotenv.2018.07.321, 2019.

Wang, S.-H., Welton, E. J., Holben, B. N., Tsay, S.-C., Lin, N.-H., Giles, D., Buntoung, S., Chantara, S., Wiriya, W., Stewart, S. A., Janjai, S., Nguyen, X. A., Hsiao, T.-C., Chen, W.-N., and Lin, T.-H.: Vertical Distribution and Columnar Optical Properties of Springtime Biomass-Burning Aerosols over Northern Indochina during 2014 7-SEAS Campaign, Aerosol and Air Quality Research, 15, 2037-2050, 10.4209/aaqr.2015.05.0310, 2015.

WHO: WHO expert consultation: available evidence for the future update of the WHO Global Air Quality Guidelines (AQGs): meeting report Bonn, Germany 29 September-1 October 2015, World Health Organization. Regional Office for Europe, 2016.

WHO: WHO global air quality guidelines: particulate matter (PM2. 5 and PM10), ozone, nitrogen dioxide, sulfur dioxide and carbon monoxide: executive summary, 2021.

Xu, L., Duan, F., He, K., Ma, Y., Zhu, L., Zheng, Y., Huang, T., Kimoto, T., Ma, T., Li, H., Ye, S., Yang, S., Sun, Z., and Xu, B.: Characteristics of the secondary water-soluble ions in a typical autumn haze in Beijing, Environ Pollut, 227, 296-305, 10.1016/j.envpol.2017.04.076, 2017.

Xue, J., Griffith, S. M., Yu, X., Lau, A. K. H., and Yu, J. Z.: Effect of nitrate and sulfate relative abundance in PM2.5 on liquid water content explored through half-hourly observations of inorganic soluble aerosols at a polluted receptor site, Atmospheric Environment, 99, 24-31,

10.1016/j.atmosenv.2014.09.049, 2014.
Yang, X., Jiang, L., Zhao, W., Xiong, Q., Zhao, W., and Yan, X.: Comparison of Ground-Based PM2.5 and PM10 Concentrations in China, India, and the U.S, Int J Environ Res Public Health, 15, 10.3390/ijerph15071382, 2018.
Yin, S., Wang, X., Zhang, X., Guo, M., Miura, M., and Xiao, Y.: Influence of biomass burning on local air pollution in mainland Southeast Asia from 2001 to 2016, Environ Pollut, 254, 112949, 10.1016/j.envpol.2019.07.117, 2019.

https://doi.org/10.5194/acp-2022-219
Preprint. Discussion started: 22 April 2022

Atmospheric Chemistry and Physics Discussions

Figure and Table

Figure 1. Location of the AERONET Sun/sky radiometer stations considered in our research work. Different colors indicate the regional locations, i.e., purple (Europe), pink (North Africa), blue (the Middle East), yellow (India), red (Southeast Asia), and green (Northeast Asia).

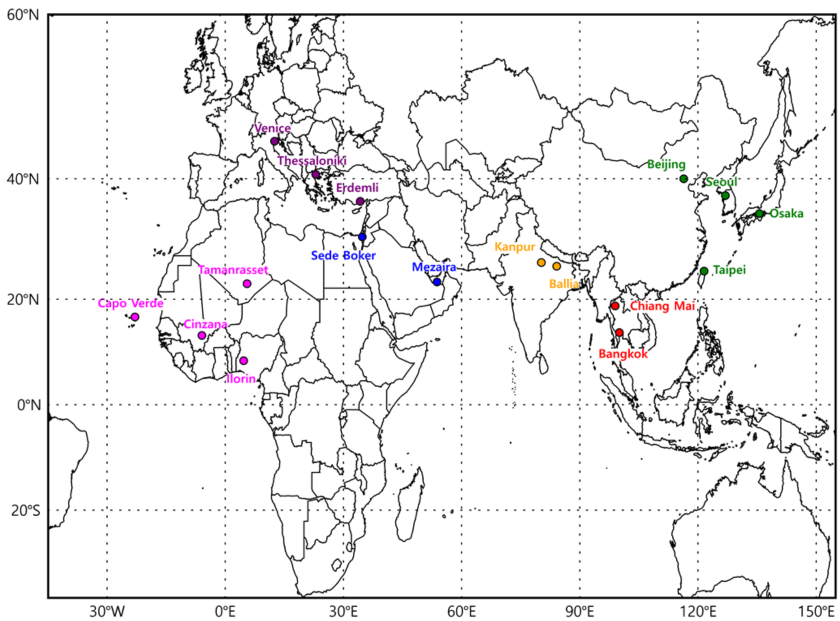

https://doi.org/10.5194/acp-2022-219
Preprint. Discussion started: 22 April 2022

Atmospheric Chemistry and Physics
Discussions

647 **Figure 2**. Aerosol type classification expressed in terms of PD (pure dust), DDM (dust dominant mixture), PDM
648 (pollution dominant mixture), and pollution aerosols, and classified in terms of NA (non-absorbing), WA (weakly
649 absorbing), MA (moderately absorbing), and SA (strongly absorbing).

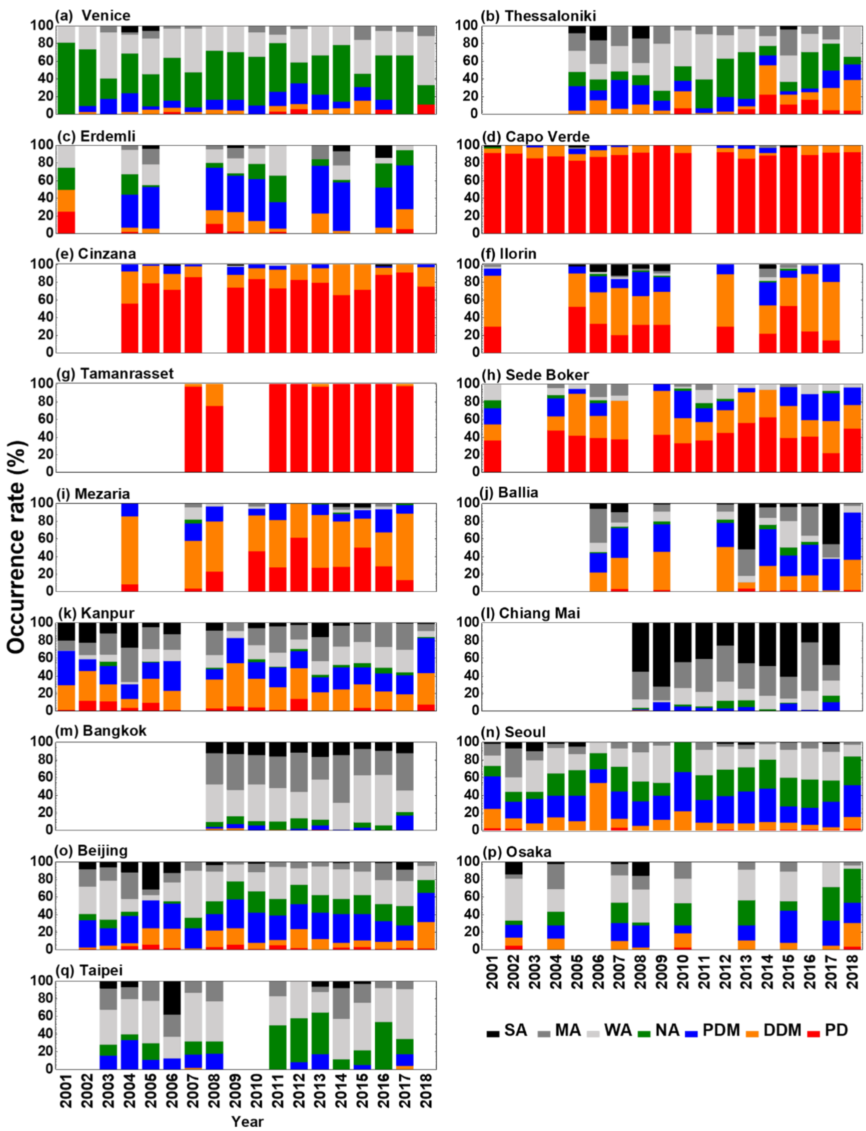

650

https://doi.org/10.5194/acp-2022-219
Preprint. Discussion started: 22 April 2022

Atmospheric Chemistry and Physics
Discussions

Figure 3. (a) Average AOD in terms of dust and coarse- and fine-mode pollution AOD, and the change of annual values of (b) total AOD (τ_T), (c) dust-only AOD (τ_D), (d) coarse-mode pollution AOD (τ_{PC}), and (e) fine-mode pollution AOD (τ_{PF}). The values inside the brackets present the percent variation for each of the 17 sites.

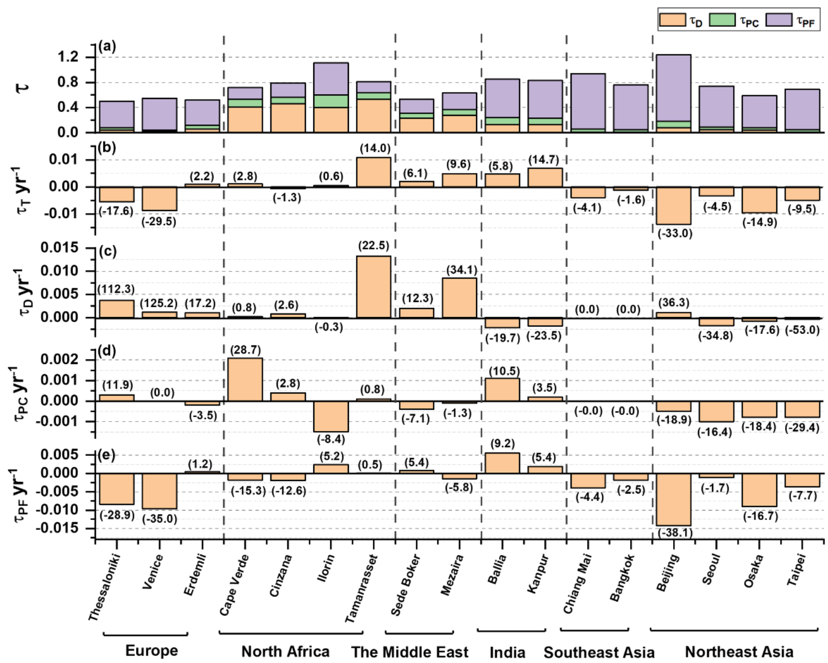

https://doi.org/10.5194/acp-2022-219
Preprint. Discussion started: 22 April 2022

Atmospheric Chemistry and Physics Discussions
Open Access
EGU

Figure 4. Average Ångström exponent (α) of (a) total and (b) fine-mode pollution particles, and the change of the annual values of the (c) total Ångström exponent (α_T) and (d) fine-mode pollution Ångström exponent (α_{PF}). The values inside the brackets present the percent variation for each of the 17 sites.

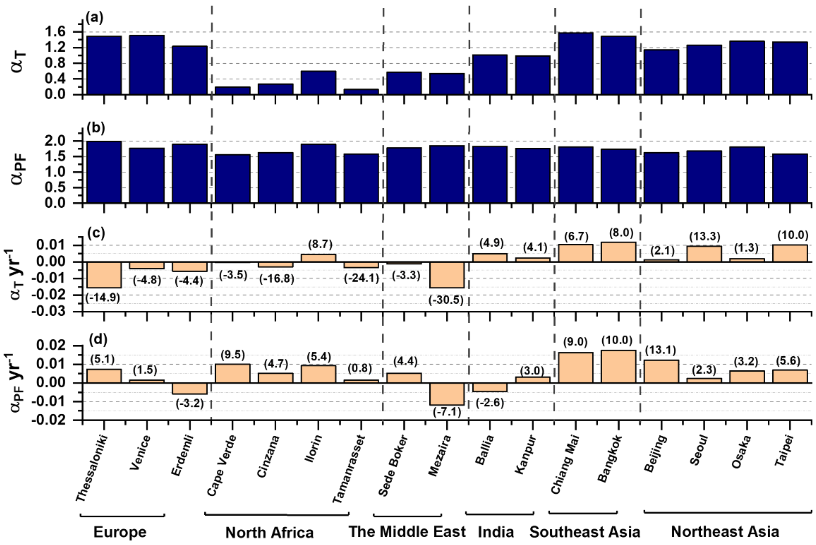

https://doi.org/10.5194/acp-2022-219
Preprint. Discussion started: 22 April 2022

Atmospheric Chemistry and Physics Discussions

Table 1. Average and standard deviation of aerosol optical depth of total (τ_T), dust (τ_D), coarse-mode particles (τ_{PC}) and fine-mode particles (τ_{PF}) at 440 nm, and Ångström exponent (440–870 nm) of total (α_T) and fine-mode particles (α_{PF}), and fine-mode fraction (FMF) for the period 2001–2018.

Site	τ_T (440 nm)	τ_D (440 nm)	τ_{PC} (440 nm)	τ_{PF} (440 nm)	α_T (440-870 nm)	α_{PF} (440-870 nm)	FMF
Thessaloniki	0.48±0.12	0.04±0.08	0.04±0.02	0.42±0.14	1.49±0.42	1.99±0.23	0.91±0.19
Venice	0.54± 0.22	0.02±0.05	0.02±0.02	0.51±0.22	1.51 ±0.28	1.77±0.27	0.96±0.14
Erdemli	0.51±0.13	0.06±0.10	0.06±0.04	0.40±0.12	1.23±0.37	1.90±0.19	0.87±0.18
Cape Verde	0.62±0.25	0.41±0.21	0.12±0.05	0.19±0.08	0.19±0.16	1.56±0.25	0.35±0.15
Cinzana	0.69±0.34	0.46±0.30	0.10±0.07	0.23±0.11	0.27±0.21	1.63±0.24	0.36±0.18
Ilorin	1.04±0.48	0.40±0.30	0.20±0.14	0.51±0.23	0.60±0.31	1.90±0.22	0.61±0.20
Tamanrasset	0.69±0.36	0.53±0.35	0.11±0.06	0.17±0.07	0.13±0.09	1.59±0.20	0.27±0.15
Sede Boker	0.49±0.20	0.23±0.22	0.08±0.05	0.22±0.09	0.57±0.43	1.78±0.27	0.56±0.28
Mezaira	0.56±0.21	0.28±0.23	0.09±0.05	0.26±0.10	0.54±0.35	1.85±0.19	0.53±0.25
Ballia	0.82±0.31	0.13±0.14	0.11±0.07	0.61±0.31	1.01±0.34	1.83±0.23	0.82±0.19
Kanpur	0.80±0.34	0.13±0.19	0.100.06	0.60±0.37	0.99±0.39	1.76±0.27	0.82±0.23
Chiang Mai	0.93±0.54	0.01±0.02	0.05±0.04	0.88±0.53	1.57±0.19	1.81±0.20	0.98±0.11
Bangkok	0.76±0.33	0.01±0.02	0.04±0.02	0.71±0.32	1.49±0.19	1.74±0.21	0.98±0.10
Beijing	1.22±0.76	0.08±0.16	0.10±0.07	1.06±0.76	1.14±0.31	1.63±0.31	0.90±0.18
Seoul	0.73±0.37	0.05±0.08	0.04±0.04	0.65±0.37	1.26±0.29	1.68±0.28	0.92±0.15
Osaka	0.58±0.21	0.04±0.08	0.04±0.02	0.51±0.21	1.36±0.31	1.81±0.22	0.92±0.14
Taipei	0.69±0.30	0.01±0.03	0.04±0.02	0.64±0.30	1.34±0.20	1.59±0.24	0.98±0.09

https://doi.org/10.5194/acp-2022-219
Preprint. Discussion started: 22 April 2022

Atmospheric Chemistry and Physics Discussions

Table 2. Change of the annual value (τyr^{-1}or yr^{-1}) and the percent variation (%) of τ_T, τ_D, τ_{PC}, τ_{PF}, FMF, α_T and α_{PF} based on the slope obtained from linear regression method. The wavelength of τ_T, τ_D, τ_{PC}, and τ_{PF} is 440 nm and that of α_T and α_{PF} ranges from 440 nm to 870 nm.

Region	Site	τ_T (% variation)	τ_D (% variation)	τ_{PC} (% variation)	τ_{PF} (% variation)	FMF (% variation)	α_T (% variation)	α_{PF} (% variation)
Europe	**Thessaloniki**	-0.0055 (-17.6)	0.0037 (112.3)	0.0003 (11.9)	-0.0084 (-28.9)	-0.0111 (-18.2)	-0.0155 (-14.9)	0.0073 (5.1)
	Venice	-0.0087 (-29.5)	0.0012 (125.2)	0.0000 (0.0)	-0.0096 (-35.0)	-0.0032 (-6.2)	-0.0040 (-4.8)	0.0015 (1.5)
	Erdemli	0.0010 (2.2)	0.0010 (17.2)	-0.0002 (-3.5)	0.0005 (1.2)	-0.0029 (-15.6)	-0.0055 (-4.4)	-0.0060 (-3.2)
North Africa	**Cape Verde**	0.0011 (2.8)	0.0002 (0.8)	0.0021 (28.7)	-0.0018 (-15.3)	-0.0025 (-11.4)	-0.0004 (-3.5)	0.0101 (9.5)
	Cinzana	-0.0006 (-1.3)	0.0008 (2.6)	0.0004 (2.8)	-0.0019 (-12.6)	-0.0018 (-4.1)	-0.0030 (-16.8)	0.0052 (4.7)
	Ilorin	0.0006 (0.6)	-0.0001 (-0.3)	-0.0015 (-8.4)	0.0024 (5.2)	0.0025 (9.4)	0.0046 (8.7)	0.0093 (5.4)
	Tamanrasset	0.0108 (14.0)	0.0133 (22.5)	0.0001 (0.8)	0.0001 (0.5)	-0.0030 (-3.7)	-0.0035 (-24.1)	0.0015 (0.8)
Middle East	**Sede Boker**	0.0020 (6.1)	0.0020 (12.3)	-0.0004 (-7.1)	0.0008 (5.4)	-0.0017 (-5.4)	-0.0012 (-3.3)	0.0052 (4.4)
	Mezaira	0.0049 (9.6)	0.0085 (34.1)	-0.0001 (-1.3)	-0.0014 (-5.8)	-0.0093 (-21.1)	-0.0157 (-30.5)	-0.0119 (-7.1)
India	**Ballia**	0.0048 (5.8)	-0.0022 (-19.7)	0.0011 (10.5)	0.0055 (9.2)	0.0046 (6.4)	0.0050 (4.9)	-0.0047 (-2.6)
	Kanpur	0.0069 (14.7)	-0.0018 (-23.5)	0.0002 (3.5)	0.0019 (5.4)	0.0032 (7.3)	0.0024 (4.1)	0.0031 (3.0)
Southeast Asia	**Chiang Mai**	-0.0039 (-4.1)	0.0000 (0.0)	-0.0000 (-0.0)	-0.0039 (-4.4)	-0.0022 (-0.9)	0.0105 (6.7)	0.0163 (9.0)
	Bangkok	-0.0012 (-1.6)	0.0000 (0.0)	-0.0000 (-0.0)	-0.0018 (-2.5)	-0.0002 (-0.1)	0.0119 (8.0)	0.0175 (10.0)
Northeast Asia	**Beijing**	-0.0138 (-33.0)	0.0011 (36.3)	-0.0005 (-18.9)	-0.0142 (-38.1)	-0.0023 (-4.6)	0.0014 (2.1)	0.0122 (13.1)
	Seoul	-0.0034 (-4.5)	-0.0017 (-34.8)	-0.0010 (-16.4)	-0.0011 (-1.7)	0.0032 (5.9)	0.0095 (13.3)	0.0024 (2.3)
	Osaka	-0.0096 (-14.9)	-0.0008 (-17.6)	-0.0008 (-18.4)	-0.0090 (-16.0)	-0.0020 (-2.1)	0.0020 (1.3)	0.0065 (3.2)
	Taipei	-0.0049 (-9.5)	-0.0004 (-53.0)	-0.0008 (-29.4)	-0.0037 (-7.7)	0.0009 (1.3)	0.0104 (10.0)	0.0069 (5.6)

https://doi.org/10.5194/acp-2022-219
Preprint. Discussion started: 22 April 2022

Atmospheric Chemistry and Physics
Discussions

Table 3. MK-test results in terms of number of data points (n), Z-value, p-value, and Sen's slope (S) of τ (440 nm) according to aerosol type. The Z-value follows the standard normal distribution and explains the significance of the trend. The p-value decides on the significance of the hypothesis (from highly likely to highly unlikely) depending on the significance level. S is Sen's slope estimator and means the degree of increase or decrease in trend. (* denotes clear trend with 95% confidence level, |z|>1.96)

Region	Site	n	τ_T			τ_D			τ_{PC}			τ_{PF}		
			Z	P	S	Z	p	S	Z	p	S	Z	p	S
Europe	**Thessaloniki**	14	**-2.5183***	0.0118	-0.0050	1.3139	0.1889	0.0034	0.2190	0.8267	0.0001	**-2.9562***	0.0031	-0.0080
	Venice	18	**-3.0302***	0.0024	-0.0084	**2.3484***	0.0189	0.0013	-0.0758	0.9396	-0.0001	**-3.3332***	0.0009	-0.0109
	Erdemli	10	0.1789	0.8580	0.0009	0.3578	0.7205	0.0006	-0.3578	0.7205	-0.0009	0.0000	1.0000	-0.0003
North Africa	**Cape Verde**	16	0.0000	1.0000	-0.0000	0.0450	0.9641	0.0002	**2.1161***	0.0343	0.0019	-1.2156	0.2241	-0.0012
	Cinzana	15	-0.0990	0.9212	-0.0011	-0.0990	0.9212	-0.0004	0.0000	1.0000	0.0002	-1.1396	0.2545	-0.0021
	Ilorin	11	-0.3114	0.7555	-0.0011	0.0000	1.0000	-0.0011	-0.4671	0.6404	-0.0035	0.0000	1.0000	0.0029
	Tamanrasset	9	1.5639	0.1179	0.0134	1.3553	0.1753	0.0135	0.7298	0.4655	0.0013	0.5213	0.6022	0.0023
Middle East	**Sede Boker**	15	0.7918	0.4285	0.0023	0.3959	0.6922	0.0026	0.0000	1.0000	-0.0000	0.4949	0.6207	0.0013
	Mezaira	11	1.0899	0.2758	0.0081	0.9342	0.3502	0.0084	-0.3114	0.7555	-0.00031	0.0000	1.0000	-0.0000
India	**Ballia**	10	0.8944	0.3711	0.0130	-0.3578	0.7205	-0.0024	0.0000	1.0000	0.00048	1.0733	0.2831	0.0188
	Kanpur	17	**2.7599***	0.0058	0.0094	-1.0298	0.3031	-0.0026	0.0000	1.0000	0.00000	**2.0184***	0.0436	0.0103
Southeast Asia	**Chiang Mai**	9	0.7298	0.4655	0.0074	-0.1789	0.8580	-0.0001	0.3578	0.7205	0.00052	0.1789	0.8580	0.0026
	Bangkok	9	**1.9809***	0.0476	0.0099	-0.5367	0.5915	-0.0002	0.0000	1.0000	-0.00001	1.0733	0.2831	0.0065
Northeast Asia	**Beijing**	16	**-2.1161***	0.0343	-0.0148	0.4953	0.6204	0.0015	-0.4953	0.6204	-0.00047	**-2.1161***	0.0343	-0.0144
	Seoul	18	-0.6818	0.4954	-0.0042	-1.3636	0.1727	-0.0012	**-2.9545***	0.0031	-0.00117	-0.6060	0.5445	-0.0029
	Osaka	9	**-3.0235***	0.0025	-0.0209	**-2.3062***	0.0211	-0.0019	**-2.3062***	0.0211	-0.00193	**-3.2320***	0.0012	-0.0206
	Taipei	13	-1.4032	0.1606	-0.0091	-0.79312	0.4277	-0.0004	-1.2812	0.2001	-0.00114	-1.1592	0.2464	-0.0076

https://doi.org/10.5194/acp-2022-219
Preprint. Discussion started: 22 April 2022

Atmospheric Chemistry and Physics Discussions
Open Access
EGU

Table 4. MK-test results in terms of number of data points (m), Z value, p-value, and Sen's slope (S) of FMF, α_T and α_{PF}. Meaning of parameters same as in Table 4. (* denotes that clear trend with 95% confidence level, |z|>1.96 and ** means clear trend with 90% confidence level, |z|>1.65)

Region	Site	n	FMF			α_T			α_{PF}		
			Z	p	S	Z	p	S	Z	p	S
Europe	**Thessaloniki**	14	**-2.1898****	0.0285	-0.0108	-1.4234	0.1546	-0.0168	1.0949	0.2736	0.0075
	Venice	18	**-2.1969****	0.0280	-0.0031	-0.9848	0.3247	-0.0058	-0.3030	0.7619	-0.0020
	Erdemli	10	-0.3578	0.7205	-0.0019	-0.3578	0.7205	-0.0087	-0.5367	0.5915	-0.0083
North Africa	**Cape Verde**	16	**-1.8459****	0.0649	-0.0028	-0.1351	0.8926	-0.0008	**2.5733***	0.0101	0.0141
	Cinzana	15	-0.5939	0.5526	-0.0013	-1.1877	0.2350	-0.0031	1.4846	0.1376	0.0073
	Ilorin	11	0.1557	0.8763	0.0027	0.1557	0.8763	0.0053	**1.8684****	0.0617	0.0115
	Tamanrasset	9	-0.7298	0.4655	-0.0033	-0.9383	0.3481	-0.0050	0.0000	1.0000	-0.0006
Middle East	**Sede Boker**	15	-0.0990	0.9212	-0.0020	0.0990	0.9212	0.0006	1.2867	0.6207	0.0075
	Mezaira	11	-0.4671	0.6404	-0.0097	-0.7785	0.4363	-0.0121	-1.5570	0.1195	-0.0203
India	**Ballia**	10	0.1789	0.8580	0.0050	0.1789	0.8580	0.0068	-0.5367	0.5915	-0.0026
	Kanpur	17	1.3594	0.1740	0.0048	0.6179	0.5366	0.0048	-0.2060	0.8368	-0.0008
Southeast Asia	**Chiang Mai**	10	0.0000	1.0000	0.0006	0.6179	0.5366	0.0128	**1.9677***	0.0491	0.0157
	Bangkok	10	0.3578	0.7205	0.0005	1.6100	0.1074	0.0120	**2.3255***	0.0200	0.0199
Northeast Asia	**Beijing**	16	-0.5939	0.5526	-0.0026	0.7654	0.4440	0.0019	**2.9265***	0.0034	0.0119
	Seoul	18	**1.6666****	0.0956	0.0021	**2.2727***	0.0231	0.0095	0.9848	0.3247	0.0022
	Osaka	9	-0.7298	0.4655	-0.0011	0.1043	0.9170	0.0006	1.1468	0.2515	0.0109
	Taipei	13	0.7931	0.4277	0.0016	**3.5995***	0.0003	0.0113	1.4032	0.1606	0.0089